Retention of NMDA receptor NR2 subunits in the lumen of endoplasmic reticulum in targeted NR1 knockout mice

Masahiro Fukaya*†, Akira Kato†‡, Chanel Lovett‡, Susumu Tonegawa‡, and Masahiko Watanabe*§

*Department of Anatomy, Hokkaido University School of Medicine, Sapporo 060-8638, Japan; and ‡Picower Center for Learning and Memory, The Howard Hughes Medical Institute, RIKEN–MIT Neuroscience Research Center, Center for Cancer Research, Departments of Biology and Brain Cognitive Sciences, Massachusetts Institute of Technology, Cambridge, MA 02139-4307

Contributed by Susumu Tonegawa, February 19, 2003

Glutamate is a major excitatory neurotransmitter in the mammalian central nervous system, and the *N*-methyl-D-aspartate-selective glutamate receptor (NR) consisting of the NR1 subunit and an NR2 or NR3 subunit plays crucial roles in synaptic transmission, plasticity, and learning and memory. By using a knockout mouse strain, in which the NR1 gene deletion is primarily targeted to the CA1 pyramidal cells of the hippocampus, we investigated the *in vivo* effect of the loss of the NR1 subunit on the cellular expression and intracellular distribution of the NR2 subunits. The NR1 gene deletion had no apparent effect on the levels of NR2A or NR2B mRNA but led to severe reductions of NR2A and NR2B protein in dendrites of CA1 pyramidal cells. This reduced dendritic distribution of the NR2 subunits accompanied their robust accumulation in perikarya, where they were condensed in the lumen of the endoplasmic reticulum as electron-dense granules. These granules were also observed in CA1 pyramidal cells of the control mice but they were much fewer and contained no detectable levels of the NR2 subunit. The effect of the NR1 knockout on intracellular localization of the NR2 subunits was specific in that no such effect was observed for the GluR1 and PSD-95, two other major postsynaptic proteins. These results suggest that the NR1 subunit plays a crucial role in the release of the NR2 subunit from the endoplasmic reticulum in hippocampal pyramidal cells *in vivo*, and when the NR1 subunit is unavailable, the NR2 subunits are retained and aggregate into intracisternal granules.

The *N*-methyl-D-aspartate (NMDA)-selective glutamate receptor (NR) is characterized by the voltage-dependent Mg^{2+} block and high Ca^{2+} permeability (1). The NMDA receptor plays multifarious roles in physiological and pathological processes in the brain, including synaptic plasticity, memory and learning, development, and excitotoxicity (2). The NMDA receptor is comprised of heterotetrameric channels consisting of the NR1 and NR2 subunits (3–5). The NR1 subunit is encoded by a single gene but exists as several variants generated by alternative splicing (6). This NR subunit is expressed in most neurons, whereas the NR2 subunits (NR2A–NR2D) are expressed in a cell-type specific manner, contributing to the functional and spatiotemporal diversities of the receptor complex (7–10). Additional subunits, NR3A and NR3B, have also been identified (11, 12). The heteromeric nature of NMDA receptors has been indicated by the demonstration that the receptors are functional only when both NR1 and NR2 subunits are introduced into *Xenopus* oocytes or cultured cells (8, 9). Further studies with the transfection of heterologous cell systems revealed that (*i*) the binding sites for the agonist glutamate and the coagonist glycine are shared between the NR1 and NR2 subunits (13, 14); (*ii*) the NR1 and NR2 subunits carry distinct roles in the intracellular trafficking, localization, and function of the receptors (15–19); and (*iii*) the NR1 and NR2 (or NR3) subunits interact in the endoplasmic reticulum (ER) as one of the early biochemical steps in the assembly of the NMDA receptors for their efficient cell surface expression (20–23).

To extend some of the studies carried out by using heterologous *in vitro* systems to a more physiological *in vivo* system, we took advantage of the NR1 knockout mice in which the deletion of the NR1 gene is targeted to the CA1 pyramidal cells of the hippocampus (CA1-NR1 knockout mice; refs. 24 and 25). Specifically, we investigated the effect of the loss of the NR1 subunit on the cellular expression and intracellular trafficking of the endogenous NR2 subunits in the CA1 pyramidal cells of the mutant mice. Here, we show that in the mutants the NR2A and NR2B subunits are nearly absent in the dendrites and accumulate in the perikarya as a form of electron-dense granules in the ER lumen. These results suggest that the NR1 subunit is indispensable for ER export of NR2 subunits *in vivo*.

Methods

Animals. We have reported the generations of the transgenic mouse line T29–1 carrying Cre recombinase under the control of the αCaMKII promoter and of the floxed NR1 (fNR1) mouse line carrying two loxP sites flanking the entire transmembrane domain and C-terminal region (exons 11–21; refs. 24 and 25). The founder mice (Cre/−, fNR1/fNR1) were crossed to homozygous fNR1 mice (−/−, fNR1/fNR1) to produce mutant (Cre/−, fNR1/fNR1) and floxed (−/−, fNR1/fNR1) littermates. For each analysis, three mutant and three floxed mice were used at a given age, except for quantitative electron microscopic analyses, which were carried out for one mutant mouse and one floxed mouse. Under deep anesthesia by pentobarbital (100 mg/kg of body weight, i.p.), brains were freshly obtained for immunoblot and *in situ* hybridization. Mice were perfused transcardially with 4% paraformaldehyde in 0.1 M sodium phosphate buffer (PB, pH 7.4) for immunoperoxidase and immunofluorescence, 4% paraformaldehyde/0.1% glutaraldehyde in 0.1 M PB for postembedding immunogold cytochemistry, and 2% paraformaldehyde/2% glutaraldehyde in 0.1 M sodium cacodylate buffer (pH 7.2) for conventional electron microscopy.

***In Situ* Hybridization.** To detect mRNAs for the mouse NMDA receptor subunits, antisense oligonucleotide probes were synthesized as follows: oligoζ1Ex11 for exon 11 of NR1 (GluRζ1) subunit cDNA (complementary to nucleotide residues 1209–1256, GenBank accession no. D10028), oligoε1L for NR2A (GluRε1) subunit cDNA (2968–3018, GenBank accession no. D10217), and oligoε2L for NR2B (GluRε2) subunit cDNA (3186–3234, GenBank accession no. D10651). Oligonucleotide probes were labeled with [^{33}P]dATP by using terminal deoxyribonucleotidyl transferase (BRL).

Abbreviations: ER, endoplasmic reticulum; ICG, intracisternal granule; IR, immunoreactivity; NMDA, *N*-methyl-D-aspartate; NR, NMDA-selective glutamate receptor.

†M.F. and A.K. contributed equally to this work.

§To whom correspondence should be addressed. E-mail: watamasa@med.hokudai.ac.jp.

NEUROSCIENCE

Fresh cryostat sections (16-μm thick) were prepared in the parasagittal plane and mounted on silane-coated glass slides. *In situ* hybridization was performed as described (26), and the specificity was confirmed by blank signals in the presence of excess unlabeled oligonucleotides. Sections were exposed either to x-ray films (Hyperfilm-β max, Amersham Pharmacia) for 2 weeks or to nuclear track emulsion (NTB-2, Kodak) for 3 weeks. For semiquantification of mRNA levels, all sections were exposed to a single x-ray film for measurement of the relative optical density with NIH IMAGE software (version 1.61).

Immunoblot. Protein samples of the whole hippocampus were prepared from each of three mutant and three floxed mice by sonication in ice-cold buffer containing 10 mM Tris·HCl (pH 7.0), 20 mM KCl, 1 mM EDTA, and 0.25 M sucrose. Protein concentration was determined by the Lowry's method. Protein samples (100 μg) were separated by SDS/7.5%/PAGE under reduced conditions and electroblotted onto a nitrocellulose membrane (Schleicher & Schuell). The membrane was immunoreacted with the following rabbit primary Abs for 1 h: NR1 (GluRζ1C) Ab (1 μg/ml), NR2A (GluRε1C) Ab (1 μg/ml), NR2B (GluRε2N) Ab (1 μg/ml), GluR1 (GluRα1C) Ab (0.5 μg/ml), and PSD-95 Ab (0.5 μg/ml), whose specificity has been reported (27–29). Immunoreaction was visualized by the enhanced chemiluminescence (ECL) detection system (Amersham Pharmacia). For semiquantification, protein bands on x-ray films were scanned to determine the relative gray level by using NIH IMAGE software.

Immunohistochemistry. We prepared paraffin sections (5 μm) for immunoperoxidase and immunofluorescence, and microslicer sections (400 μm) for postembedding immunogold. Before primary Ab incubation, all sections except for postembedding immunogold were pretreated with pepsin (1 mg/ml, DAKO) in 0.2 M HCl at 37°C for 10 min. All immunohistochemical incubations were performed at room temperature. For immunoperoxidase, sections immunoreacted overnight with primary Ab to NR1, NR2A, NR2B, GluR1, or PSD-95 (0.5–1 μg/ml) were visualized by the avidin-biotin-peroxidase method with 3,3′-diaminobenzidine. Without pepsin pretreatment, no significant immunoreaction was obtained, as reported (27–29). The specificity of immunohistochemical signals was confirmed by negative staining when the primary Abs were preabsorbed with antigen peptides (30–100 μg/ml). For double immunofluorescence, sections were incubated with rabbit NR2A or NR2B Ab and with goat calreticulin or cathepsin D Ab (1:500 for each, Santa Cruz Biotechnology) overnight, followed by FITC- or Cy3-labeled species-specific secondary Abs for 2 h (1:200, Jackson ImmunoResearch). Immunoreaction was observed by a confocal laser-scanning microscope (Fluoview, Olympus, Tokyo).

For postembedding immunogold, microslicer sections were cryoprotected with 30% glycerol in PB and frozen with liquid propane in a cryofixation unit (CPC, Leica). The specimens were transferred to 0.5% uranyl acetate in methanol in a cryosubstitution unit (AFS, Leica), and embedded in Lowicryl HM20 resin (Lowi, Waldkraiburg, Germany). Ultrathin sections on nickel grids were immunoreacted overnight with NR2A or NR2B Ab (10 μg/ml) and then with colloidal gold (15 nm) conjugated with anti-rabbit IgG (British Biocell International, Cardiff, U.K.) for 2 h. Grids were stained with 2% uranyl acetate for 10 min. The number of immunogolds was counted on profiles of asymmetrical axo-spinous synapses or intracisternal granules (ICGs) in the CA1 region. By using IPLAB software (Nippon Roper, Tokyo), the distribution of gold particles was evaluated as the distance from the center of ICGs to the center of gold particles, and as the distance from the limiting membrane of ER to the center of gold particles.

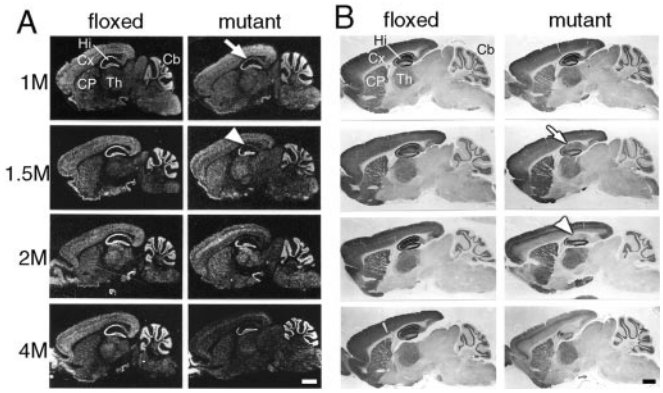

Fig. 1. Age-dependent NR1 knockout in the CA1-NR1 knockout mouse. (*A*) *In situ* hybridization with antisense NR1 probe. Photographs are negative images printed directly from x-ray films. (*B*) Immunoperoxidase with NR1 Ab. Pairs of floxed and mutant brains were embedded in single paraffin blocks to be processed simultaneously. Arrows and arrowheads indicate the hippocampal CA1 region at stages when NR1 reduction is first observed or reaches the lowest level, respectively. 1M–4M, 1–4 months of age; Cb, cerebellum; CP, caudate-putamen; Cx, cortex; Hi, hippocampus; Th, thalamus. (Bars = 1 mm.)

Results

Spatial Restriction of NR1 Knockout in the CA1-NR1 Knockout Mouse Is Age-Dependent. We first examined in detail the age dependency of the distribution of NR1 knockout in the mutant (CA1-NR1 knockout) mice by *in situ* hybridization (Fig. 1*A*) and immunohistochemistry (Fig. 1*B*). In the control (floxed) brains, relatively high levels of NR1 mRNA and NR1 immunoreactivity (IR) were detected in the hippocampus, neocortex, caudate-putamen, thalamus, and cerebellar granular layer throughout the animals' ages. In the brains derived from 1-month-old mutants, the levels of NR1 mRNA were reduced specifically in the hippocampal CA1 and subiculum (white arrow in Fig. 1*A*). At 1½ months of age, the mRNA disappeared almost entirely in these regions (white arrowhead in Fig. 1*A*). The spatial distribution of NR1 IR in 1-month-old mutants was indistinguishable from that of control littermates but at 1½ months of age, the IR levels in the mutant were reduced substantially and rather specifically in the CA1 and subiculum compared with the controls of the matching age (white arrow in Fig. 1*B*). The IR levels of the mutants in these hippocampal regions further decreased at 2 months of age, reaching the lowest level observed throughout the age groups (arrowhead in Fig. 1*B*). However, at 2 months of age, the reduction of the NR1 IR level in the mutants relative to controls was also observed in other areas, most conspicuously in the deep layer of the neocortex (Fig. 1*B*). The reduction of NR1 mRNA was also observed in the deep cortical layers of 2-month-old mutant mice. As the mutants grew older, the NR1 knockout extended to other telencephalic regions: in the CA3 region and deep cortical layers at 2–4 months of age and the dentate gyrus at 4 months of age. In contrast, no reduction of NR1 mRNA or IR levels was observed in the thalamus, cerebellar granular layer, or hippocampal CA2 region through the age groups.

These data suggest that the spatial distribution of NR1 knockout is highly age-dependent. Up to sometime between 1½ and 2 months of age, the knockout is relatively restricted to the CA1 and subiculum of the hippocampus as the earlier study suggested (24, 25) but in older mice the knockout spreads to other telencephalic areas. In the further study, we used mutants and control littermates of 2 months of age.

Normal Transcription Levels of Hippocampal NR2 Subunits. In the adult hippocampus, the NR2A and NR2B subunits are coexpressed with the NR1 subunit (7–10, 26). We examined the effect

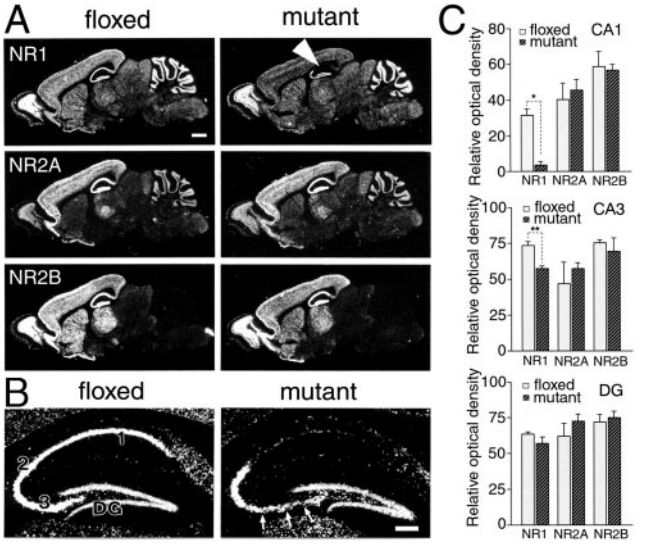

Fig. 2. Transcription levels of NR1, NR2A, and NR2B mRNAs in the hippocampus at 2 months of age. (*A*) X-ray film autoradiography for NR1 (*Top*), NR2A (*Middle*), and NR2B (*Bottom*) mRNAs using adjacent parasagittal brain sections. Note normal expressions of NR2A and NR2B mRNAs in the mutant CA1 region, in contrast to virtual disappearance of NR1 mRNA (white arrowhead). (*B*) Emulsion-dipped microautoradiography for NR1 mRNA. Arrows indicate a slight reduction of NR1 mRNA in the CA3 region. (*C*) Semiquantification of x-ray film autoradiograms to compare transcription levels in the CA1 region (*Top*), CA3 region (*Middle*), and dentate gyrus (DG, *Bottom*). The mean and SDs were calculated from three floxed or three mutant mice. 1–3, CA1–CA3 regions. *, $P < 0.001$; **, $P < 0.01$. [Bars = 1 mm (*A*) and 0.1 mm (*B*).]

of NR1 knockout on the levels of NR2A and NR2B. The level of NR1 mRNA in the mutant CA1 region (white arrowhead in Fig. 2*A*) was reduced to 10% of that in the control CA1 region (Fig. 2*C Top*; Student's *t* test, $P < 0.001$, $n = 3$). The remaining signals in the CA1 region were attributable to putative interneurons, judging from dispersed intrahippocampal distribution (Fig. 2*B*). In the CA3 region, particularly in the area close to the dentate gyrus (arrows in Fig. 2*B*), a slight reduction was observed in the level of NR1 mRNA (79% of the control CA3; Fig. 2*C Middle*, $P < 0.01$) but no significant reduction was seen in the dentate gyrus (Fig. 2*C Bottom*, $P > 0.05$). We examined the levels of NR2A and NR2B mRNAs in the hippocampal sections immediately adjacent to those used for the examination of the NR1 mRNA and found no indication of an effect of the NR1 knockout (Fig. 2 *A* and *C*, $P > 0.05$ for all).

Reduced Protein Levels of Hippocampal NR2 Subunits. At the protein level, the contents of the three NR subunits were investigated by immunoblot with the whole hippocampal homogenates (Fig. 3*A* and *B*). As expected, protein levels of the NR1 subunit in the mutant hippocampus were significantly reduced to 28% of the levels in the control hippocampus (*t* test, $P < 0.05$, $n = 3$). Unexpectedly, protein levels of the NR2A and NR2B subunits in the mutant hippocampus were both reduced to 65% of those in the control hippocampus ($P < 0.05$ for each). No such reduction was noted for PSD-95, a scaffolding molecule that interacts with the NR2A and NR2B subunits in the postsynaptic density (15) or for the GluR1 subunit of the α-amino-3-hydroxy-5-methyl-4-isoxazole propionic acid (AMPA)-type glutamate receptor (Fig. 3 *A* and *B*). Thus, the NR1 knockout does not seem to affect the levels of the NR2 mRNAs but selectively reduces their protein contents in the hippocampus.

Altered Intracellular Localization of NR2 Subunits. We examined the effect of the NR1 knockout on the intracellular distribution of

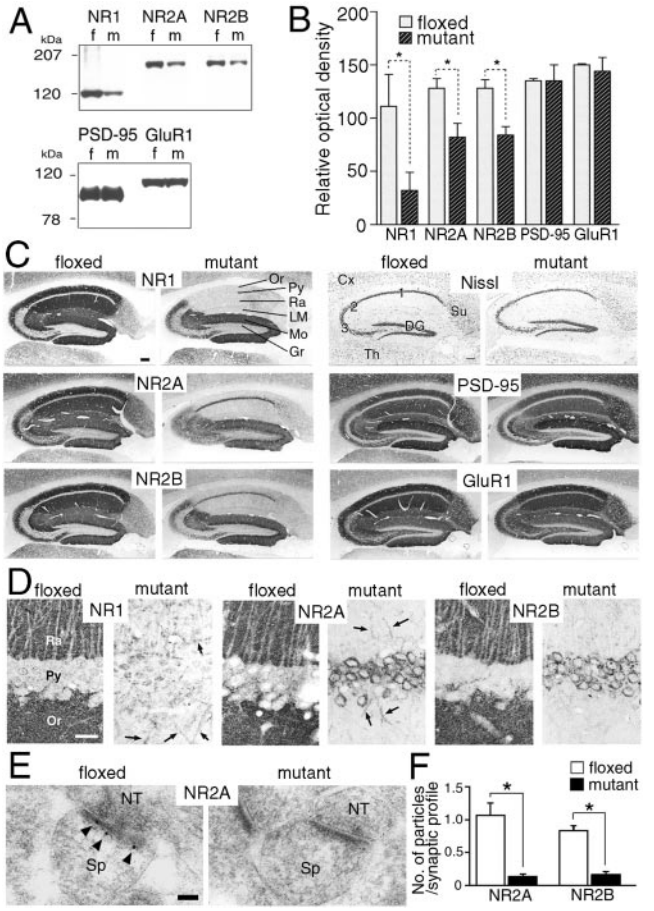

Fig. 3. Immunoblot and immunohistochemistry for NR1, NR2A, NR2B, PSD-95, and GluR1 in the hippocampus at 2 months of age. (*A*) Immunoblot using the whole hippocampal protein extracts from floxed (f) and mutant (m) mice. (*B*) The relative optical density of immunoblot protein bands. Significant reductions are observed for NR1, NR2A, and NR2B subunits (*, $P < 0.05$ for each). Similar results were obtained with x-ray films of different exposure times, indicating the detection within the linear range of signal intensity. (*C*) Histology and immunohistochemistry. (*D*) High-power views of immunostained CA1 region. Note a dense accumulation of NR2A and NR2B subunits in perikarya of mutant pyramidal cells, in contrast to almost negative labeling in those of the floxed cells. Arrows indicate immunopositive dendritic shafts of putative interneurons. (*E*) Postembedding immunogold staining for NR2A subunit at asymmetrical axo-spinous synapses of floxed and mutant CA1 region. Note the lack of gold labeling in the mutant synapse, in contrast to postsynaptic labeling in the floxed one (arrowheads). (*F*) The number of immunogold particles per profile of asymmetrical axo-spinous synapses in the CA1 region of the floxed (white bars) and mutant (black bars) mice. Immunogold labeling is significantly reduced for both NR2A and NR2B subunits (*, $P < 0.01$). Cx, cortex; DG, dentate gyrus; Gr, granule cell layer; LM, stratum lacunosum-moleculare; Mo, stratum moleculare; NT, nerve terminal; Or, stratum oriens; Py, pyramidal cell layer; Ra, stratum radiatum; Sp, spine; Su, subiculum; Th, thalamus; 1–3, CA1–CA3 regions. [Bars = 0.1 mm (*C*), 20 μm (*D*), and 100 nm (*E*).]

the NR2A and NR2B subunits in the CA1 pyramidal cells. Nissl staining revealed no obvious abnormalities in the laminar architecture, cellular density, or cellular arrangement in the mutant hippocampus (Fig. 3*C*). Immunohistochemical staining with NR1 Ab indicated that NR1 IRs were specifically and greatly reduced in the whole regions of the mutant CA1 compared with the control CA1 (Fig. 3 *C* and *D*). Interestingly, NR2A and NR2B epitopes were also nearly absent in the dendritic layers (strata oriens, radiatum, and lacunosum-moleculare) of the mutant CA1 (Fig. 3 *C* and *D*). By postembedding immunogold,

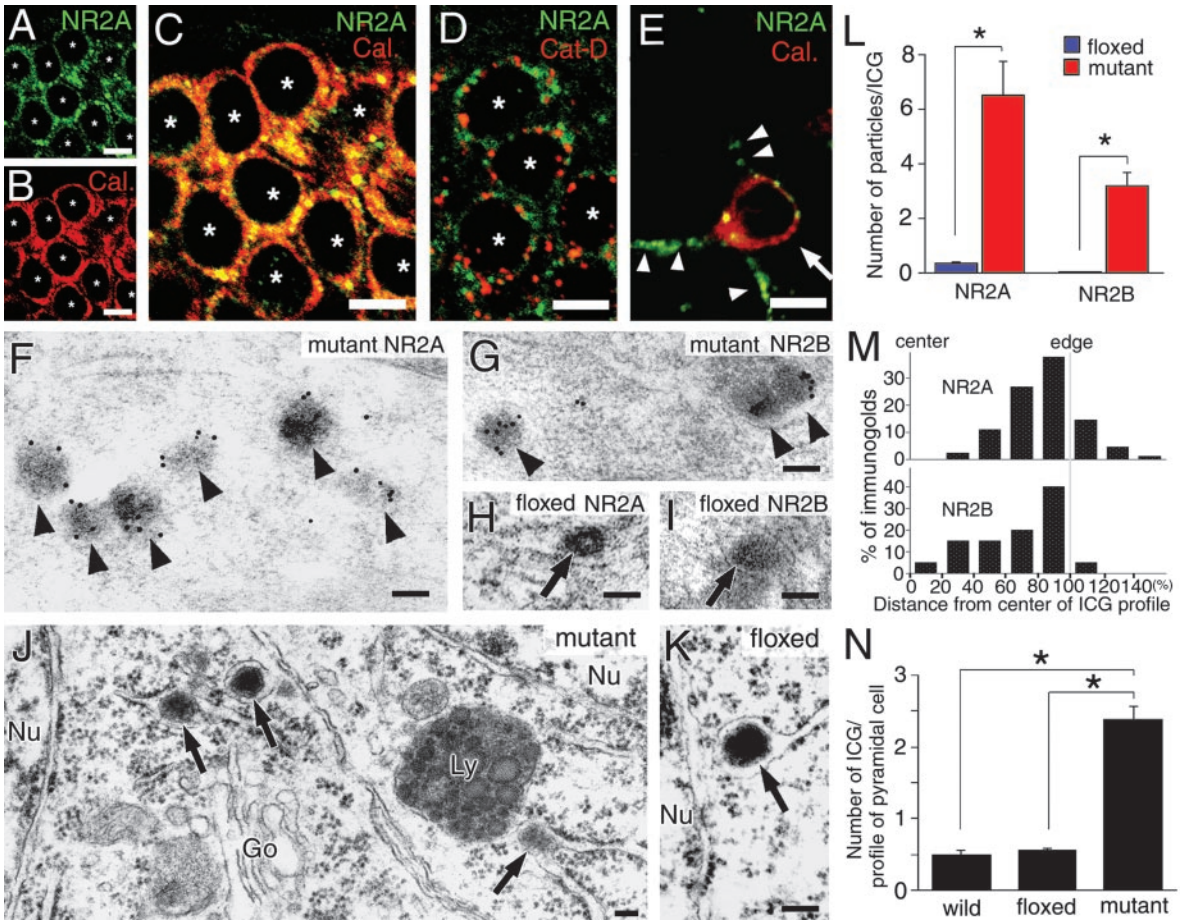

Fig. 4. Immunofluorescence and electron microscopic analyses demonstrating ER retention of NR2 subunits in mutant CA1 pyramidal cells at 2 months of age. (*A–D*) Double immunofluorescence for NR2A (green) and ER marker calreticulin (Cal., red) or lysosomal marker cathepsin D (Cat-D, red) in mutant CA1 pyramidal cells. White asterisks indicate the nucleus of pyramidal cells. (*E*) Double immunofluorescence for NR2A (green) and Cal. (red) in a mutant CA1 interneuron (white arrow). NR2A subunit is detected as tiny puncta along the surface of the cell body and dendritic processes of this interneuron (white arrowheads). (*F–I*) Postembedding immunogold labeling for the NR2A (*F* and *H*) and NR2B (*G* and *I*) subunits in CA1 pyramidal cells of the mutant (*F* and *G*) and floxed (*H* and *I*) hippocampi. Black arrowheads and arrows indicate immunogold-positive or -negative granules in the ER, respectively. (*J* and *K*) Conventional electron microscopy showing the presence of electron-dense granules (black arrows) in the ER lumen of CA1 pyramidal cell perikarya in mutant (*J*) and floxed (*K*) mice. (*L*) The number of NR2A and NR2B immunogold particles per profile of ICGs in CA1 pyramidal cells of the floxed (blue bars) and mutant (red bars) mice (*, $P < 0.01$). (*M*) Histograms for the central-to-peripheral distribution of immunogold particles for the NR2A (*Upper*) and NR2B (*Lower*) subunits on ICG profiles in the mutant CA1 pyramidal cells. The scores of 0% and 100% indicate the center or edge of electron-dense ICGs, respectively, and the distance from the center of ICGs to the center of gold particles is plotted as 20% wide bins. (*N*) The number of ICGs per pyramidal cell profile on electron micrographs in the C57BL (wild), floxed, and mutant mice (*, $P < 0.01$). Go, Golgi apparatus; Ly, lysosome; Nu, nucleus. [Bars = 10 μm (*A–E*) and 100 nm (*F–K*).]

gold particles representing the NR2 subunits were detected on the postsynaptic membrane of asymmetrical synapses in the control CA1, whereas they were very rare in the mutant CA1 (Fig. 3*E*). When quantified, the number of gold particles per profile of asymmetrical axo-spinous synapses in the CA1 region was severely and significantly reduced in the mutant mice to 12% (NR2A) or 19% (NR2B) of that in the control mice (Fig. 3*F*; *t* test, $P < 0.01$ for each, $n = 30$ synapses). Furthermore, this specific disappearance of NR2 epitopes in the CA1 dendrites of the mutants was accompanied with the greatly increased appearance of NR2 IRs in the perikarya of the CA1 pyramidal cells (Fig. 3 *C* and *D*). We also examined the distribution of PSD-95 and GluR1 in the mutant hippocampus and found no indication of the effect of the NR1 knockout (Fig. 3*C*).

These results suggest that the NR1 subunit plays a crucial role in the trafficking of the NR2 subunit from perikarya to the postsynapse. In the mutant CA1 region, residual NR2 IRs were observed in a few irregularly oriented dendritic shafts (Fig. 3*D*), presumably, dendrites of hippocampal interneurons.

Accumulation of NR2 Subunits in the ER Lumen. We investigated the site of somatic accumulation of the NR2 subunits in the mutant hippocampal CA1 region. In double immunofluorescence staining experiments, signals for the NR2A (Fig. 4*A*, green) and NR2B (data not shown) subunits were observed as punctate or reticular labelings within pyramidal cell perikarya. The intensity of immunofluorescence was greater in punctate than reticular structures. Surface labeling of neuronal cell bodies was not evident. Ab to calreticulin (Fig. 4*B*, red), an ER resident protein (30), also labeled the perikarya. When merged, the two types of fluorescence overlapped well in pyramidal cell perikarya, yielding a yellowish color on punctate structures and an orange color on reticular structures (Fig. 4*C*). On the other hand, immunolabeling for the NR2A (Fig. 4*D*, green) and NR2B (data not shown) was separated from immunofluorescence for lysosomal enzyme cathepsin D (Fig. 4*D*, red), suggesting that punctate labeling represents NR2 subunit accumulation in the ER but not in lysosomes. In interneurons, somatic accumulation of the NR2 subunits was not observed, and NR2 IRs were detected as tiny

puncta along the surface of cell bodies and dendrites (arrowheads in Fig. 4*E*), suggesting normal cell surface expression.

According to immunogold staining, the NR2 subunits in the pyramidal cell perikarya of the mutants were mostly localized to electron-dense granules (Fig. 4 *F* and *G*). These labeled granules were enclosed by the limiting membrane, which was often continuous to ribosome-attached ER (i.e., rER), but the membrane itself was scarcely labeled for the NR2 subunits. No significant gold labeling was detected in the Golgi apparatus and cell membrane of the CA1 pyramidal cells of mutants. By conventional electron microscopy, such dense granules were confirmed to exist in the lumen of rER or its extended sac lacking ribosomes (i.e., sER) in the mutant pyramidal cells (arrows in Fig. 4*J*). ICGs were also encountered in CA1 pyramidal cells of floxed (Fig. 4*K*) and C57BL wild-type (data not shown) mice. In these controls, however, NR2 IRs were hardly detected in ICGs (Fig. 4 *H* and *I*; *L*, $P < 0.001$ for NR2A and NR2B, *t* test, $n = 20$ granules). Moreover, ICGs were less frequently encountered in the controls compared with the mutant: the number of ICGs per neuronal profile was 24% and 17% of that in the mutant (Fig. 4*N*; $P < 0.01$ for each, *t* test, $n = 50$ pyramidal cells). These results demonstrate that in the absence of the NR1 subunit, the NR2 subunits are retained in pyramidal cell perikarya and condensed in electron-dense granules within the ER lumen.

Detailed distribution in ICGs was analyzed for the NR2A and NR2B subunits. In the center-to-edge axis of ICGs, many immunogold particles were located peripherally, peaking at the most peripheral region (80–100% bin), while they were few in the central region (0–20% bin) or outside of ICGs (>100% bins) (Fig. 4*M*, $n = 102$ particles for the NR2A, $n = 82$ particles for the NR2B). We also measured the distance from the limiting membrane of ER to immunogold particles [it was 36.6 ± 2.6 nm for the NR2A subunit and 49.3 ± 4.3 nm for the NR2B subunit (mean $\pm$ SE)]. These results indicate that NR2 IRs are preferentially detected in the periphery of ICGs apart from the ER membrane.

In the mutant (Fig. 4*J*) and control (data not shown) mice, lysosomes in the CA1 pyramidal cells contained a number of electron-dense granules. These lysosomal granules varied in size but the largest one was almost similar in size to ICGs (50–150 nm in diameter). In both mice, no significant gold labeling for the NR2A or NR2B subunit was seen in the lysosomal granules (data not shown).

Discussion

In the CA1-NR1 knockout mouse, hippocampal contents of the NR2A and NR2B subunits were reduced, although there was no indication of a reduction in their mRNA levels. Immunohistochemistry demonstrated that the NR2A and NR2B subunits disappeared from pyramidal cell dendrites and synapses in the mutant CA1. Reciprocally, the levels of somatic NR2 subunits were much higher in the mutant cells compared with the control cells, due to their accumulation in the ER. These results suggest that the NR2 subunits are translated but are unable to exit the ER when the NR1 subunit is unavailable.

Stringent NR1-Dependent Quality Control Mechanism in the ER. Transfection studies indicated that the NR2A and NR3A subunits form complexes with the NR1 subunit in the ER, and that this kind of complex formation is necessary for their exit from the ER and cell surface expression (20, 21, 23). Our work extended these findings made by using *in vitro* techniques and heterologous cell lines to an *in vivo* study with a homologous cell system (i.e., hippocampal CA1 pyramidal cells). Such an extension is important because the cellular and biochemical mechanisms controlling expression, subunit assembly, intracellular trafficking, cell surface expression, and synaptic localization of heterooligomeric cell surface receptors are complex, and it is quite possible that they differ in different types of cells and under different conditions. We demonstrate here that the NR1 subunit is indispensable for suppressing ER retention of the NR2 subunits *in vivo*. The requirement of the NR1 subunit for the ER exit of the NR2 subunits is in line with the notion that a quality control mechanism operates in the ER for a transport of various multisubunit membrane proteins to the plasma membrane (31, 32).

It is known that post-ER steps for the functioning of NMDA receptors, including dendritic transport, synaptic localization and trafficking, and functional diversity, are regulated by the NR2 subunits or through their specific interaction with other dendritic and postsynaptic proteins (8, 9, 13–19, 33–35). The present finding that the NR2A and NR2B subunits are virtually lost from dendrites and synapses, and robustly accumulated in the somatic ER in NR1-deficient pyramidal cells, demonstrates that the NR1-dependent quality control in the ER is highly stringent and its passage through the ER is a prerequisite for all known subsequent NR2-dependent processes. This stringent NR1-dependent mechanism seems to be consistent with findings that the intracellular pool of the NR2 subunits is much smaller than that of the NR1 subunit in cultured neurons (36, 37).

ICG Formation of ER-Retained NR2 Subunits. Our data showed that NR2 subunits retained in the absence of the NR1 subunit are accumulated as a form of electron-dense granules in the ER lumen. It has been shown that secretory proteins aggregate into granules within the ER when their synthesis is overstimulated or their secretory pathway is blocked (38–40). Our finding extends these phenomena to cell membrane proteins. The retained NR2 subunits are likely to lose their native topology and integration into the ER membrane, because cytoplasmic (C terminus of the NR2A subunit) and luminal (N terminus of the NR2B subunit) epitopes are both detected in ICGs. This notion is supported further by the finding that measured distance from the ER membrane to gold particles (36.6 nm for NR2A and 49.3 nm for NR2B) exceeds the estimated maximum distance from epitopes to the center of immunogold particles with a diameter of 15 nm (41). These granules are not an artifact of the genetic manipulation because they are also found, albeit in a fewer number, in the CA1 pyramidal cells of control mice. We propose that ICGs are a natural subcellular component in which a variety of misfolded or misassembled proteins produced through normal processes is condensed for degradation. Although NR2 IRs were hardly detected in the ICGs of control mice, this result may simply reflect the sensitivity of the detection method used. When the NR1 gene is knocked-out, the production of retained NR2 subunits increases strikingly in the ER, which then facilitates the formation of ICGs and elevates contents of NR2 IRs in individual ICGs.

Possible Fate of ICGs. A prevailing hypothesis on the major fate of secretory and membrane proteins retained in the ER is intracytosolic degradation by the 26S proteasome (42–44). When the formation of retained proteins exceeds the capacity of proteasomal degradation, these proteins form huge electron-dense aggregates called aggresomes. Examples are for cystic fibrosis transmembrane conductance regulator (CFTR) and presenilin-1 (45). It is possible that NR2 subunits retained in ICGs undergo similar proteasomal degradation and aggresome formation. However, whereas aggresomes are membraneless structures formed in the cytoplasm, the NR2-containing granules are membrane-bound structures in the ER lumen. Thus, if the NR2 subunits condensed as ICGs are to be degraded through the cytoplasmic ubiquitin–proteasomal pathway, they will have to be retrotranslocated from the ER to the cytoplasm before degradation. It is unlikely that the ICGs of about 50–150 nm in diameter *per se* will undergo this retrotranslocation.

NR2 IRs were preferentially detected in the periphery of ICGs. Because epitopes are evenly exposed on the section surface in the postembedding immunogold technique, it is unlikely that the peripheral-to-central gradient of NR2 IRs was due to uneven Ab penetration and accessibility to the epitopes. Rather, it is likely that unassembled NR2 subunits were pulled off from the ER membrane to the surface of ICGs, where they undergo ER-associated degradation, a form of proteolysis distinct from lysosomal degradation (46). Then, NR2 subunits lose their IRs and are condensed as the core of ICGs. The present finding that lysosomes contain numerous electron-dense granules with sizes and electron densities similar to those of ICGs (Fig. 4*J*) seems worthy to note as a possible fate of ICGs. Although NR2 IRs are not detected in the lysosomal granules, this result could be due to the loss of NR2 IRs through ER-associated degradation, and the remnant of ICGs may be processed for terminal digestion in lysosomes. It is necessary to confirm this scheme of NR2 processing in the absence of NR1 with additional experiments.

In summary, our study shows that the NR1 subunit is indispensable for ER exit of NR2 subunits *in vivo*, and the lack of the NR1 subunit leads to retention of the NR2 subunits in the ER lumen as electron-dense granules. Our data also suggest a degradation route of retained membrane proteins that is distinct from the prevailing view.

This work was supported in part by a Grant-in-Aid for Special Coordination Funds for Promoting Science and Technology and for Scientific Research on Priority Areas from the Ministry of Education, Culture, Sports, Science, and Technology of Japan (to M.W.); by the Research Fellowships of the Japan Society for the Promotion of Science for Young Scientists (to M.F.); by National Institute of Mental Health Center Grant PH50-MH58880 (to S.T.); and by a gift from the Shionogi Institute for Medical Science (to S.T.).

1. Mayer, M. L. & Westbrook, G. L. (1987) *J. Physiol. (London)* **394,** 501–527.
2. Bliss, T. V. & Collingridge, G. L. (1993) *Nature* **361,** 31–39.
3. Seeburg, P. H. (1993) *Trends Neurosci.* **16,** 359–365.
4. Nakanishi, S. & Masu, M. (1994) *Annu. Rev. Biophys. Biomol. Struct.* **23,** 319–348.
5. Mori, H. & Mishina, M. (1995) *Neuropharmacology* **34,** 1219–1237.
6. Sugihara, H., Moriyoshi, K., Ishii, T., Masu, M. & Nakanishi, S. (1992) *Biochem. Biophys. Res. Commun.* **185,** 826–832.
7. Kutsuwada, T., Sakimura, K., Manabe, T., Takayama, C., Katakura, N., Kushiya, E., Natsume, R., Watanabe, M., Inoue, Y., Yagi, T., *et al.* (1996) *Neuron* **16,** 333–344.
8. Meguro, H., Mori, H., Araki, K., Kushiya, E., Kutsuwada, T., Yamazaki, M., Kumanishi, T., Arakawa, M., Sakimura, K. & Mishina, M. (1992) *Nature* **357,** 70–74.
9. Monyer, H., Sprengel, R., Schoepfer, R., Herb, A., Higuchi, M., Lomeli, H., Burnashev, N., Sakmann, B. & Seeburg, P. H. (1992) *Science* **256,** 1217–1221.
10. Watanabe, M., Inoue, Y., Sakimura, K. & Mishina, M. (1992) *NeuroReport* **3,** 1138–1140.
11. Ciabarra, A. M., Sullivan, J. M., Gahn, L. G., Pecht, G., Heinemann, S. & Sevarino, K. A. (1995) *J. Neurosci.* **15,** 6498–6508.
12. Nishi, M., Hinds, H., Lu, H., Kawata, M. & Hayashi, Y. (2001) *J. Neurosci.* **21,** RC185.
13. Hirai, H., Kirsch, J., Laube, B., Betz, H. & Kuhse, J. (1996) *Proc. Natl. Acad. Sci. USA* **93,** 6031–6036.
14. Laube, B., Hirai, H., Sturgess, M., Betz, H. & Kuhse, J. (1997) *Neuron* **18,** 493–503.
15. Kornau, C., Schenker, L. T., Kennedy, M. B. & Seeburg, P. H. (1995) *Science* **269,** 1737–1740.
16. Niethammer, M., Kim, E. & Sheng, M. (1996) *J. Neurosci.* **16,** 2157–2163.
17. Wyszynski, M., Lin, J., Rao, A., Nigh, E., Beggs, A. H., Craig, A. M. & Sheng, M. (1997) *Nature* **385,** 439–442.
18. Ehlers, M. D., Fung, E. T., O'Brien, R. J. & Huganir, R. L. (1998) *J. Neurosci.* **18,** 720–730.
19. Setou, M., Nakagawa, T., Seog, D. H. & Hirokawa, N. (2000) *Science* **288,** 1796–1802.
20. McIlhinney, R. A., Molnar, E., Atack, J. R. & Whiting, P. J. (1996) *Neuroscience* **70,** 989–997.
21. McIlhinney, R. A., Le Bourdelles, B., Molnar, E., Tricaud, N., Streit, P. & Whiting, P. J. (1998) *Neuropharmacology* **37,** 1355–1367.
22. Okabe, S., Miwa, A. & Okado, H. (1999) *J. Neurosci.* **19,** 7781–7792.
23. Pérez-Otaño, I., Schulteis, C. T., Contractor, A., Lipton, S. A., Trimmer, J. S., Sucher, N. J. & Heinemann, S. F. (2001) *J. Neurosci.* **21,** 1228–1237.
24. Tsien, J. Z., Chen, D. F., Gerber, D., Tom, C., Mercer, E. H., Anderson, D. J., Mayford, M., Kandel, E. R. & Tonegawa, S. (1996) *Cell* **87,** 1317–1326.
25. Tsien, J. Z., Huerta, P. T. & Tonegawa, S. (1996) *Cell* **87,** 1327–1338.
26. Watanabe, M., Inoue, Y., Sakimura, K. & Mishina, M. (1993) *J. Comp. Neurol.* **338,** 377–390.
27. Watanabe, M., Fukaya, M., Sakimura, K., Manabe, T., Mishina, M. & Inoue, Y. (1998) *Eur. J. Neurosci.* **10,** 478–487.
28. Fukaya, M. & Watanabe, M. (2000) *J. Comp. Neurol.* **426,** 572–586.
29. Yamada, K., Fukaya, M., Shimizu, H., Sakimura, K. & Watanabe, M. (2001) *Eur. J. Neurosci.* **13,** 2025–2036.
30. Peter, F., Nguyen, V. P. & Soling, H. D. (1992) *J. Biol. Chem.* **267,** 10631–10637.
31. Green, W. N. & Millar, N. S. (1995) *Trends Neurosci.* **18,** 280–287.
32. Ellgaard, L., Molinari, M. & Helenius, A. (1999) *Science* **286,** 1882–1888.
33. Mori, H., Manabe, T., Watanabe, M., Satoh, Y., Suzuki, N., Toki, S., Nakamura, K., Yagi, T., Kushiya, E., Takahashi, T., *et al.* (1998) *Neuron* **21,** 571–580.
34. Steigerwald, F., Schulz, T. W., Schenker, L. T., Kennedy, M. B., Seeburg, P. H. & Kohr, G. (2000) *J. Neurosci.* **20,** 4573–4581.
35. Barria, A. & Malinow, T. (2002) *Neuron* **35,** 345–353.
36. Hall, R. A. & Soderling, T. R. (1997) *J. Biol. Chem.* **272,** 4135–4140.
37. Huh, K. H. & Wenthold, R. J. (1999) *J. Biol. Chem.* **274,** 151–157.
38. Carrell, R. & Travis, J. (1985) *Trends Biochem. Sci.* **10,** 20–24.
39. Arias, A. E. & Bendayan, M. (1993) *Eur. J. Cell Biol.* **62,** 282–293.
40. Ozawa, H. (1991) *Cell Tissue Res.* **263,** 405–412.
41. Matsubara, A., Laake, J. H., Usami, S. & Ottersen, O. L. (1996) *J. Neurosci.* **16,** 4457–4467.
42. Brodsky, J. L. & McCracken, A. A. (1997) *Trends Cell Biol.* **7,** 151–155.
43. Kopito, R. R. (1997) *Cell* **88,** 427–430.
44. Plemper, K. R. & Wolf, D. H. (1999) *Trends Biochem. Sci.* **24,** 266–270.
45. Johnston, J. A., Ward, C. L. & Kopito, R. R. (1998) *J. Cell Biol.* **143,** 1883–1898.
46. Klausner, R. D. & Sitia, R. (1990) *Cell* **62,** 611–614.